INDC(IND)*21/R

B.A.R.C.-279

B.A.R.C.-279

सत्यमेव जयते

GOVERNMENT OF INDIA
ATOMIC ENERGY COMMISSION

EVALUATION OF NEUTRON CROSS SECTIONS ON THE BASES OF OPTICAL AND STATISTICAL MODELS.

by

S. B. Garg, K. Balasubramanian and V. K. Shukla
Reactor Engineering Division

BHABHA ATOMIC RESEARCH CENTRE
BOMBAY, INDIA
1967

B.A.R.C.-279

B.A.R.C.-279

GOVERNMENT OF INDIA
ATOMIC ENERGY COMMISSION

EVALUATION OF NEUTRON CROSS SECTIONS ON THE BASES OF OPTICAL AND STATISTICAL MODELS ..

by

S.B. Garg, K. Balasubramanian and V.K. Shukla
Reactor Engineering Division

BHABHA ATOMIC RESEARCH CENTRE
BOMBAY, INDIA
1967

CONTENTS

TABLES

ABSTRACT

In order to produce accurate calculation of the neutronics of reactors, precise knowledge of inelastic and elastic cross sections and their angular distributions is desired. Optical model and Hauser-Feshbach theory have been used to compute total, elastic and inelastic cross sections of several materials which are of special interest from the point of view of a reactor physicist. These calculations also serve to test the validity of these two nuclear models which are frequently used in the continuum energy region. In general, the calculated total cross section agrees well with the measured one. The data presented herein will be incorporated into multi-group computer codes for reactor analysis. Strength functions can also be calculated on the basis of optical model.

INTRODUCTION

Optical model was developed by Feshbach et al[2] to explain the giant resonances in total neutron cross sections of a large number of nuclei observed by Barschall et al[4]. The broad maxima in cross sections cannot be explained on the basis of compound nucleus mechanism since the compound nucleus states are long-lived thereby necessitating narrow resonances and small widths. The shell model, which reduces the many body interaction between the target and the projectile to a two body one through a real potential, predicts widely spaced resonances and slow change of the cross sections with energy quite contrary to the experiment. The optical model combines in it the merits of strong coupling model (compound nucleus) and weak coupling model (shell model) and falls in between the two. Here the interaction potential is given by

$$V(r) = -Vc(r) - U(r) - i\,W(r) - V_{SO}(r) \quad \text{..................(1)}$$

Where $Vc(r)$ is the Coulomb potential, usually taken to be that due to a uniformly charged sphere of radius R, for neutrons it is zero. $U(r)$ and $W(r)$ are the real and imaginary parts of the central potential and account for refraction and absorption of neutrons in the target nucleus. The imaginary part leads to the formation of a compound nucleus and its magnitude determines the width of resonance. $V_{SO}\,(r)$ is the spin orbit potential and is responsible for the polarisation of the scattered particles.

This model is valid when the interaction averages over a large number of resonances in the compound system. In practice this occurs when the energy of the incident particle is high enough for there to be many energy levels. At lower energies, where the interaction goes through one or a few resonances, or when one inelastic channel dominates the interaction, the model is not valid.

The inelastic scattering of neutrons is treated by Hauser-Feshbach theory[1] which is based on statistical model of the compound nucleus. The compound elastic scattering contributions are also obtainable by this method.

Theory :

Only the outline of the broad features of optical and statistical models would be given below.

The exact form of the optical potential given in (1) is

$$V(r) = -Uf(r) - iWg(r) - V_{SO}\,h(r)\,l\cdot\sigma \quad \text{------} \quad (2)$$

Where the real part has a Saxon form

$$f(r) = \left[1 + \exp\left(\frac{r-R}{a}\right)\right]^{-1} \quad \text{------} \quad (3)$$

The imaginary part has a Gaussian form

$$g(r) = \mathrm{Exp}\left[-\left(\frac{r-R}{b}\right)^2\right] \quad \text{------} \quad (4)$$

and the spin dependent part has a Thomas form

$$h(r) = \left[\frac{\hbar}{\mu_\pi c}\right]^2 \frac{1}{r}\,\frac{df(r)}{dr} \quad \text{------} \quad (5)$$

The Coulomb potential term has been dropped for the case of neutrons.

Now the cross section for reaction X (a, b) Y is given by[3,9]:

$$X(a,b)Y = \sigma_{CN}(a)\,G_c(b) \quad \text{------} \quad (6)$$

Where $G_c(b)$ is the probability for the particular mode of decay and $\sigma_{CN}(a)$ is the cross section for the formation of compound nucleus given by :

$$\sigma_{CN}(a) = \pi \lambda\!\!\!^{-2} \sum_{l,j} (2l+1)\,T_{lj} \quad \text{------} \quad (7)$$

Where T_{lj} are the transmission coefficients given by

$$T_{lj} = 1 - |\eta_{lj}|^2 \quad \text{------} \quad (8)$$

η_{lj} is the relative amplitude of the outgoing wave and is obtained by the solution of the Schrödinger equation with complex potential given by (2).

$\eta_{lj} = e^{i\delta_{lj}}$, δ_{lj} , being the phase shifts (9)

The calculation of the T_{lj} is thus dependent on η_{lj} which is further governed by several factors :

(1) The real and imaginary parts of the logarithmic derivative f_{lj} of the radial wave functions.

(2) The shift factor $S_{\ell j}$ which gives a measure of the level shift due to extra-nuclear interaction.

(3) The penetration factor $P_{\ell j}$ which gives a measure of the probability of the ℓ^{th} partial wave penetration of the centrifugal angular momeutum barrier.

$$T_{\ell j} = \frac{-4 P_{\ell j} \, Im(f_{\ell j})}{[Re\, f_{\ell j} - S_{\ell j}]^2 + [Im\, f_{\ell j} - P_{\ell j}]^2} \quad \text{-------} (10)$$

The quantity $\eta_{\ell j}$ is the essential feature of reaction cross section calculations, it also completely determines the shape elastic scattering cross section through the well-known relationship.

$$\sigma_{sc}(\theta)\, d\Omega = \pi \lambda\!\!\!^{-2} \left[\sum (2\ell+1)(1-\eta_{\ell j}) \frac{P_\ell(\cos\theta)}{\sqrt{4\pi}} \right]^2 d\Omega \quad \text{----} (11)$$

Eqn. (11) is employed in optical model analysis in which the primary objective is to determine the optical model parameters which best fit experimental data by numerically solving the radial wave equation, thereby determining the logarithmic derivative $f_{\ell j}$ and hence $\eta_{\ell j}$. The criterion to obtain the best fit is to determine best parameters which minimise the function.

$$x^2 = \sum_{i=1}^{N} \left[\frac{\sigma_{th}(\theta_i) - \sigma_{exp}(\theta_i)}{\Delta \sigma_{exp}(\theta_i)} \right]^2 \quad \text{--------} (12)$$

where $\sigma_{th}(\theta_i)$ is the theoretical differential cross section and $\Delta \sigma_{exp}(\theta_i)$ is an experimental error.

Optical model would predict total, shape elastic and compound nucleus formation cross sections.

$$\sigma_t = \sigma_{se} + \sigma_{CN} \quad \text{--------------} (13)$$

Hauser-Feshbach Statistical Model

The Hauser-Feshbach model[1,5] is based on the statistical assumption that all states of the compound nucleus which are accessible on the basis of conservation of energy, angular momentum and parity do participate, but that formation and decay take place in an incoherent manner. A consequence of this is that all angular distributions of scattered particles are symmetric about 90°. The extent to which this is satisfied by the data is a measure of the validity of the assumption.

Hauser and Feshbach considered $T_{\ell}(E)$ to be a function of ℓ only. The total cross section for the scattering of neutrons of incident energy E by a nucleus with a ground state having spin I_0 and parity π_0 to produce outgoing neutrons of energy E' leaving the residual nucleus in a state with energy E_q having spin I_q and parity π_q is given by :

$$\sigma(E,E') = \frac{\pi \lambda^2}{2(2I_0+1)} \sum_{\ell} T_{\ell}(E) \sum_{J} \frac{\epsilon_{j\ell J}(2J+1) \sum_{\ell' j'} \epsilon_{j'\ell' J} T_{\ell'}(E')}{\sum_{p\ell'' j''} \epsilon_{j''\ell'' J} T_{\ell''}(E'_p)} \quad \text{---(}$$

Where the sum over p in the denominator is taken over all accessible levels $E_p < E$ including the ground state E_0 $(E'_p = E - E_p)$, the ℓ' and ℓ'' sums run over all values which lead to final states consistent with parity conservation.

$$(-1)^{\ell'} \pi_q = (-1)^{\ell} \pi_0 , \qquad (-1)^{\ell''} \pi_p = (-1)^{\ell} \pi_0$$

and j's are the channel spins and take on values

$$j_{1,2} = I_0 \pm \tfrac{1}{2}, \quad j'_{1,2} = I_q \pm \tfrac{1}{2} \text{ and } j''_{1,2} = I_p \pm \tfrac{1}{2}$$

$$\epsilon_{j\ell J} = \left\{ \begin{array}{l} 2 \text{ if both } j_1 \text{ and } j_2 \\ 1 \text{ only one of } j_1 \text{ and } j_2 \\ 0 \text{ neither } j_1 \text{ nor } j_2 \end{array} \right\} \qquad \text{satisfy } |J-\ell| \leq j_i \leq (J+\ell)$$

and J takes on values

$$|\ell - j_i| \leq J \leq (\ell + j_i)$$

The angular distribution has the form

$$\sigma(E,E',\theta) = \frac{\lambda^2}{4}\cdot\frac{1}{2(2I_0+1)}\sum_{l} T_l(E) \sum_{J} \frac{\epsilon_{jlJ}\sum_{l'j'}\epsilon_{j'l'J}\,T_{l'}(E_q')}{\sum_{pl''j''}\epsilon_{j''l''J}\,T_{l''}(E_p')} \quad \text{---- (15)}$$
$$\times \sum_{L\,\mathrm{even}} \left| Z(lJlJ, jL)\, Z(l'Jl'J, j'L)\, P_l(\cos\theta)\right|$$

Where $L \leq \min(2l, 2l', 2J)$ and $Z(abcd, ef)$ are the Z-coefficient of Blatt and Bieden-harn. If dependence of transmission coefficient on j is accounted for and the channel spin notation is dropped in favour of one which considers the total neutron angular **momentum**, expressions analogous to (14) and (15) are obtained as follows:

$$\sigma(E,E') = \frac{\pi\lambda^2}{2(2I_0+1)} \sum_{lj} T_{lj}(E) \sum_{J} \frac{(2J+1)\sum_{j'l'} T_{l'j'}(E')}{\sum_{pj''l''} T_{l''j''}(E_p')} \quad \text{--- (14a)}$$

$$\sigma(E,E',\theta) = \frac{\lambda^2}{4}\cdot\frac{1}{2(2I_0+1)} \sum_{jl} T_{lj}(E) \sum_{J} \frac{(2J+1)^2 \sum_{j'l'} T_{l'j'}(E')}{\sum_{pj''l''} T_{l''j''}(E_p')}$$
$$\times \sum_{L\,\mathrm{even}} (-1)^{I-I'}\, Z(l'j'l'j', \tfrac{1}{2}L)\, Z(ljlj, \tfrac{1}{2}L)$$
$$\times\, W(Jj'Jj', I'L)\, W(JjJj, IL)\, P_l(\cos\theta) \quad \text{--- (15a)}$$

Here J, j', j'' satisfy the relations

$$|I_0 - j| \leq J \leq (I_0 + j)\ ; \quad |J - I_q| \leq j' \leq (J + I_q)$$
$$|J - I_p| \leq j'' \leq (J + I_p)$$

l's satisfy the relations $l = j \pm \frac{1}{2}$ and

$$(-1)^{l'}\,\Pi_q = (-1)^{l}\,\Pi_0\ ; \quad (-1)^{l''}\,\Pi_p = (-1)^{l}\,\Pi_0$$

Compound elastic scattering contributions are obtained by letting $E' = E$, $I_q = I_0$ and $\Pi_q = \Pi_0$ in equations (14.a) and (15.a).

Calculations

We have made optical model analysis of neutrons having energy between 0.1 and 4.0 MeV and elastically scattered on Cr-52, Ni-58, Ni-60, Th-232 and U-238. The total scattering cross section have been taken either from BNL-325 or from KFK-120 and we have assigned an error of 10% in the data since these measurements were made about a decade ago. The local optical model parameters U, W, V_{SO}, r, a and b are adjusted to give the best fit to the measured differential elastic scattering cross section and these are then utilized in the prediction of the total cross-section. The calculated total cross-section is then directly comparable to the measured one.

In the present analysis we have varied r and W to get a best fit while keeping all other parameters fixed. To test the accuracy of the model and computer code ABACUS-2[7] we have used the parameters of Moore and Auerbach to calculate the total and differential elastic scattering cross sections of Th-232 and U-238. We have issued tables of differential elastic cross sections at various energies so that they can be used to compute $\bar{\mu}$ -the average cosine of the scattering angle in the laboratory system and hence the transport cross section which is required in diffusion theory calculations of reactors.

Ni^{58} and Ni^{60}

Ni^{58} constitutes 67.85% and Ni^{60} 26.22% of natural nickel. It is imperative to know the nuclear behaviour of each of these two isotopes since nickel is one of the constituents of stainless steel which finds a frequent usage as a structural material in nuclear reactors. The parameters U = 45.0 MeV; a = 0.5 fm and V_{SO} = 0 were kept fixed in the whole range 0.1 to 4.0 MeV which is sub-divided into the following four parts to obtain the best values of r and W :-

(i) $(0.1 \leq E \leq 0.5$ MeV)	W = 18.0 MeV; r = 1.45 fm
(ii) $(0.5 < E \leq 1.5$ MeV)	W = 5.0 MeV; r = 1.45 fm
(iii) $(1.5 < E \leq 3.5$ MeV)	W = 5.0 MeV; r = 1.35 fm
(iv) (E = 4.0 MeV)	W = 4.0 MeV; r = 1.35 fm

These parameters were used to calculate differential elastic and total cross sections. Saxon-Woods form of central potential was used both for real and imaginary parts. The measured and calculated total cross sections have been compared in Table I. In the energy range 0.1 to 0.5 MeV the total cross section of Ni^{58} shows some fluctuations and it is not always possible to obtain sufficiently energy-averaged data to make optical model calculations which are meaningful in the fluctuating regions. However, our calculations represent the general trend very well if viewed on the average basis in the range 0.1 to 0.5 MeV. The agreement between measured and calculated total cross sections is almost complete in the range 0.5 to 4.0 MeV. In the energy range $0.5 < E \leq$ 1.5 MeV, we studied the effect of variation of W on the total cross section by keeping the r fixed at 1.35 fm and found that total cross section increased slowly with W but did not show an agreement with the measured one. It indicated that a slight increase in the cross section was due to the fact that more pronounced levels were included while taking the average but to account for all levels which had $\Gamma \sim D$ it was necessary to vary r. Variation of r did improve the agreement. As the energy of the incident beam of neutrons increases, the levels of the compound nucleus tend to form a continuum i.e. $\Gamma > D$. In this region variation of r does not make a significant contribution and both r and W can be suitably adjusted to give best results.

To determine compound elastic and inelastic scattering cross sections we have taken the ~~following~~ energy levels, their spins and parities from the nuclear data sheets.

Ni-58

Energy level (MeV)	J^{π}
0.0	0^+
1.452	2^+
2.458	4^+ (2^+)

Ni-60

Energy level (MeV)	J^{π}
0.0	0^+
1.332	2^+
2.158	2^+
2.502	4^+
2.627	2^+
3.130	2^+
3.523	2^+

The exact prediction of inelastic scattering cross sections is dependent on the precise knowledge of the energy levels, their spins and parities. If any energy level is not resolved, it would affect the calculated result. Thus in the case of Ni-58 inelastic cross sections above 3.0 MeV should be taken qualitatively rather than quantitatively. We have calculated inelastic cross sections of 2.458 level with J^{π} as 4^+ and 2^+ and found that cross section for 2^+ was higher. It is so because it is easier to excite low J levels. Compound elastic cross section should decrease with an increase in energy since the number of channels increase. The calculations support it. Also since the scattering takes place only after the formation and decay of compound nucleus except for the direct or shape elastic, it has to be symmetric about 90° in the centre of mass system. All these phenomena have been well represented in the calculations. Ni^{60} has not been extensively measured from cross section point of view. Our calculations serve to provide some information to those who are involved in nuclear data work. The calculated cross-sections for these two isotopes are tabulated in Tables 1 to 6 and the variations of σ_t with energy and W are shown graphically in Figs. 1 to 5.

Chromium-52

It is also a constituent of stainless steel and as such needs a better representation in the cross section studies. The optical model parameters U, a and V_{SO} have been taken to be the same as for Ni and the energy range 0.5 to 4.0 MeV has been broken up into two parts for r and W :

(i) (E = 0.5 MeV) W = 6.0 MeV; r = 1.45 fm

(ii) ($0.5 < E \leq 4.0$ MeV) W = 4.0 MeV; r = 1.45 fm

We have not attempted to calculate cross sections below 0.5 MeV since there are large fluctuations and their representation would be more difficult on the basis of optical model. The calculated and measured cross sections are recorded in Table 7 and it can be inferred that the calculated results are within the experimental error. We have studied the effect of variation of r and W on the total cross section and found that it was not very sensitive to the change in W but the change in r made significant differences. These studies indicate that fitting of parameters to data for one nucleus or even perhaps for a few nuclei can hardly give a potential which is adequate to describe data for a large number of nuclei. This is expected since the observed differences in parameters ought to correlate with the details of nuclear structure, such as the nuclear size and shape, the texture of the surface, the effects of closed shells and of nuclear spin.

We have used the following energy levels to compute inelastic scattering cross sections.

Energy level (MeV)	J^{π}
0	0^+
1.46	2^+
2.43	4^+
2.965	2^+
3.112	6^+

The shape of angular distributions is dependent on UR^2 and Wb and so an agreement can always be struck by varying either U or R and keeping all other parameters fixed; or by varying W and b in such a way that Wb = constant. The change of nuclear surface diffuseness has a marked effect on the shape of angular distributions. Thus various possible combinations can be worked out which fit in the measured elastic distributions. The only disadvantage of such a process sometimes is that one has to put forward a new set of parameters for each energy point but it is always possible though laborious to optimise it and obtain average parameters which give a good representation of scattering phenomena in a certain energy range. The calculated results are shown in Tables 7 to 9. Figs. 6 and 7 represent the variation of σ_t with energy and $\mathcal{P}$ at a fixed W respectively.

Th^{232} and U^{238}

We have checked the calculations of Moore and Auerbach using the same parameters and energy levels and found that our adapted code was correct. We studied the effect of variation of spin orbit term in potential and concluded that this part of the potential mainly affected the polarizations without making any significant contribution to the total and reaction cross sections. The energy levels and parameters used in calculations are given below :-

Th^{232}

$U=41.3$ MeV; $W=7.28$ MeV;
$V_{SO}=7.0$ MeV; $r = 1.32$ Fm;
$a = 0.47$ Fm; $b = 1.0$ Fm.

Energy level (MeV)	J^{π}
0	0^+
0.05	2^+
0.163	4^+
0.330	6^+
0.725	0^+
0.775	2^+
0.788	2^+
0.838	3^+
0.875	4^+
1.045	1^-
1.095	3^-

U^{238}

$U=39.8$ MeV; $W=6.9$ MeV;
$V_{SO}= 15.0$ MeV; $r = 1.32$ Fm;
$a = 0.47$ Fm; $b = 1.0$ Fm.

Energy level (MeV)	J^{π}
0	0^+
0.045	2^+
0.148	4^+
0.308	6^+
0.651	1^-
0.710	3^-
0.728	5^-
0.935	0^+
0.986	2^+
1.03	2^+
1.11	3^+
1.13	4^+
1.17	4^+

Tables 10 to 16 record σ_t, σ_{in}, σ_e, differential elastic scattering and neutron excitation cross-sections to different levels.

CONCLUSIONS

We have used spherical optical model with local potential to calculate these rather few cases and based on this meagre data we conclude that it is possible to find average parameters which contain structural information of the interacting nuclei and give good fits to the measurements. These parameters can then be employed to predict elastic distributions, total and reaction cross sections in those energy regions where no measurements have been made. By fitting the data at a number of energy points the dependence of parameters on energy can be approximately known and the data can then be extra-polated or interpolated to compute cross sections at other energy points. This type of calculation gives results within 10% or 15%. However, to get very reliable results it is better to switch over to non-local optical model potentials and deformed optical model in the case of deformed nuclides and include the effects of width distributions. We propose to undertake these studies in the future.

Hauser-Feshbach theory with a resonable set of level assignments reproduces the general experimental features quite well. We would be able to say more about these two models in future when we have extensively used them.

ACKNOWLEDGEMENTS

Thanks are due to Shri H.K. Bhatia for many helpful discussions and Shri P.V. Suryanarayanan for helping us with the figures. We also express our sincere thanks to Dr. E.H. Auerbach and Miss Frances Pope of Brookhaven National Laboratory (U.S.A) for making their code ABACUS-2 available to us.

REFERENCES

1. W. Hauser and H. Feshbach; Phys.Rev. 87, 366 (1952)
2. H. Feshbach et al; Phys.Rev. 96, 448 (1954)
3. P.A. Moldauer; Nucl. Phys. 47, 65 (1963)
4. H.H. Barschall; Phys.Rev. 86, 431 (1952)
5. E.H. Auerbach and S.O. Moore; Rev. 135, B895 (1964)
6. B. Buck and F. Perey; Nucl. Phys. 32, 353 (1962)
7. E.H. Auerbach; BNL - 6562 - ABACUS -2 Code
8. A.B. Smith; Phys. Rev. 126, 718 (1962)
9. P.E. Hodgson; The optical model of elastic scattering
10. D.J. Hughes and J.A. Harvey; BNL - 325
11. M.D. Goldberg et al; BNL - 400
12. J.J. Schmidt; KFK - 120

Table 1

Ni-58

E_n (MeV)	σ_t(b) KFK - 120	σ_t(b) Calculated	σ_e(b)	σ_{in}(b)
0.1	7.86 ± 10%	5.07	5.07	-
0.2	5.65 ± 10%	4.49	4.49	-
0.3	5.0 ± 10%	4.25	4.25	-
0.4	2.55 ± 10%	4.06	4.06	-
0.5	3.83 ± 10%	3.91	3.91	-
0.7	3.48 ± 10%	3.59	3.59	-
0.8	3.42 ± 10%	3.50	3.50	-
1.0	3.34 ± 10%	3.38	3.38	-
1.5	3.25 ± 10%	3.24	2.95	0.29

Ni-58

E_n (MeV)	σ_t(b)	
	KFK - 120	Calculated
2.0	3.21 ± 10%	3.22
2.5	3.20 ± 10%	3.32
3.0	3.33 ± 10%	3.34
3.5	3.39 ± 10%	3.36
4.0	3.45 ± 10%	3.47

* Corresponds to 2.458 (2^+) level.

σ_e(b)	σ_{in}(b)
2.69	0.53
2.64	0.67
2.57, 2.50*	0.77, 0.84*
2.50, 2.43*	0.86, 0.93*
2.60, 2.53*	0.87, 0.94*

Table 2

Ni-58

Calculated Cross-Sections (barns) for Neutron Excitation of Ni-58

E_n (MeV)	Compound Elastic	Excited levels (MeV)	
		1.452	2.458
0.1	1.871	-	-
0.2	1.527	-	-
0.3	1.447	-	-
0.4	1.382	-	-
0.5	1.291	-	-
0.7	1.493	-	-
0.8	1.465	-	-
1.0	1.419	-	-
1.5	1.043	0.293	-

Table 2 continued

Calculated Cross-Sections (barns) for Neutron Excitation of Ni-58

E_n (MeV)	Compound Elastic	Excited levels (MeV)	
		1.452	2.458
2.0	0.778	0.530	-
2.5	0.661	0.674	-
3.0	0.536, 0.460*	0.740, 0.628*	0.031, 0.218*
3.5	0.426, 0.351*	0.755, 0.640*	0.101, 0.292*
4.0	0.338, 0.273*	0.718, 0.603*	0.154, 0.334*

* Corresponds to 2.458 (2^+) level.

Table 3

Ni-58

Differential Elastic Cross-Sections of Ni-58 $\frac{(\text{barns})}{\text{Sr}}$

COS Ø c.m.	Energy (MeV)								
	0.1	0.2	0.3	0.4	0.5	0.7	0.8	1.0	1.5
+1.0	0.499	0.515	0.563	0.599	0.633	0.678	0.718	0.799	0.948
0.9	0.484	0.491	0.525	0.550	0.573	0.578	0.601	0.648	0.721
0.8	0.470	0.469	0.491	0.506	0.519	0.495	0.505	0.526	0.543
0.7	0.457	0.448	0.460	0.466	0.471	0.427	0.427	0.428	0.406
0.6	0.445	0.430	0.430	0.430	0.429	0.371	0.363	0.350	0.303
0.5	0.434	0.410	0.404	0.397	0.391	0.325	0.312	0.290	0.228
0.4	0.424	0.393	0.380	0.368	0.357	0.288	0.272	0.245	0.176
0.2	0.405	0.363	0.338	0.319	0.301	0.236	0.217	0.186	0.121
0.0	0.390	0.337	0.305	0.280	0.258	0.204	0.185	0.158	0.107
-0.2	0.378	0.316	0.279	0.250	0.226	0.188	0.172	0.150	0.114
-0.4	0.370	0.301	0.260	0.230	0.207	0.185	0.173	0.157	0.129
-0.5	0.367	0.295	0.254	0.223	0.201	0.190	0.179	0.166	0.137
-0.6	0.364	0.290	0.249	0.219	0.198	0.198	0.190	0.179	0.147
-0.7	0.363	0.286	0.247	0.218	0.199	0.212	0.206	0.198	0.158
-0.8	0.363	0.284	0.247	0.220	0.203	0.233	0.229	0.223	0.172
-0.9	0.363	0.283	0.250	0.226	0.211	0.261	0.260	0.257	0.191
-1.0	0.364	0.283	0.256	0.235	0.224	0.298	0.301	0.302	0.217

Table 3 continued

Differential Elastic Cross-Sections of Ni-58 $\left(\frac{\text{barns}}{\text{Sr}}\right)$

cos ø c.m.	Energy (MeV) 2.0	2.5	3.0	3.5	4.0
+1.0	0.969	1.147	1.297	1.454	1.682
0.9	0.750	0.850	0.929	0.990	1.118
0.8	0.574	0.619	0.648	0.656	0.708
0.7	0.434	0.441	0.438	0.420	0.432
0.6	0.325	0.308	0.287	0.258	0.249
0.5	0.241	0.211	0.181	0.152	0.134
0.4	0.178	0.142	0.111	0.086	0.067
0.2	0.099	0.067	0.044	0.031	0.024
0.0	0.063	0.043	0.033	0.029	0.030
-0.2	0.053	0.044	0.043	0.044	0.050
-0.4	0.063	0.058	0.057	0.058	0.060
-0.5	0.074	0.069	0.064	0.062	0.060
-0.6	0.091	0.083	0.073	0.066	0.057
-0.7	0.113	0.101	0.084	0.070	0.055
-0.8	0.143	0.125	0.100	0.076	0.057
-0.9	0.183	0.159	0.124	0.089	0.068
-1.0	0.234	0.205	0.160	0.112	0.095

Table 4

Ni-60

E_n (MeV)	σ_t (b)	σ_e (b)	σ_{in} (b)
0.1	5.13	5.13	-
0.2	4.55	4.55	-
0.3	4.30	4.30	-
0.4	4.11	4.11	-
0.5	3.96	3.96	-
0.7	3.66	3.66	-
0.8	3.56	3.56	-
1.0	3.41	3.41	-
1.5	3.23	2.80	0.43

Table 4 continued

Ni-60

E_n (MeV)	σ_t(b)	σ_e(b)
2.0	3.29	2.67
2.5	3.37	2.54
3.0	3.39	2.42
3.5	3.39	2.35
4.0	3.50	2.46

	σ_{in}(b)
	0.62
	0.83
	0.97
	1.04
	1.04

Table 5

Ni-60

Calculated Cross-Sections (barns) for Neutron Excitation of Ni-60

E_n (MeV)	Compound Elastic	Excited levels (MeV)					
		1.332	2.158	2.502	2.627	3.130	3.523
0.1	1.872	—	—	—	—	—	—
0.2	1.532	—	—	—	—	—	—
0.3	1.454	—	—	—	—	—	—
0.4	1.390	—	—	—	—	—	—
0.5	1.349	—	—	—	—	—	—
0.7	1.442	—	—	—	—	—	—
0.8	1.410	—	—	—	—	—	—
1.0	1.360	—	—	—	—	—	—
1.5	0.846	0.431	—	—	—	—	—

Table 5 continued

Calculated Cross Sections (barns) for Neutron Excitation of Ni-60

		Excited levels (MeV)					
E_n (MeV)	Compound Elastic	1.332	2.158	2.502	2.627	3.130	3.523
2.0	0.765	0.619	-	-	-	-	-
2.5	0.551	0.631	0.202	-	-	-	-
3.0	0.367	0.558	0.261	0.019	0.124	-	-
3.5	0.242	0.465	0.272	0.060	0.169	0.075	-
4.0	0.158	0.365	0.254	0.080	0.175	0.102	0.058

Table 6

Ni-60

Differential Elastic Cross-Sections of Ni-60 $(\frac{\text{barns}}{\text{Sr}})$

COS ø c.m.	Energy (MeV)								
	0.1	0.2	0.3	0.4	0.5	0.7	0.8	1.0	1.5
+1.0	0.506	0.523	0.573	0.609	0.644	0.686	0.722	0.797	0.906
0.9	0.491	0.499	0.534	0.559	0.583	0.586	0.607	0.648	0.691
0.8	0.476	0.476	0.498	0.514	0.528	0.504	0.511	0.528	0.521
0.7	0.463	0.455	0.466	0.473	0.479	0.435	0.433	0.431	0.390
0.6	0.451	0.435	0.436	0.436	0.435	0.379	0.370	0.354	0.292
0.5	0.439	0.416	0.409	0.403	0.397	0.333	0.319	0.294	0.220
0.4	0.429	0.399	0.385	0.373	0.362	0.296	0.279	0.249	0.169
0.2	0.410	0.367	0.342	0.323	0.305	0.243	0.223	0.191	0.117
0.0	0.394	0.341	0.308	0.283	0.261	0.210	0.192	0.163	0.104
-0.2	0.382	0.320	0.281	0.252	0.229	0.194	0.177	0.155	0.111
-0.4	0.373	0.304	0.262	0.232	0.208	0.190	0.178	0.161	0.124
-0.5	0.370	0.297	0.256	0.225	0.202	0.194	0.183	0.169	0.131
-0.6	0.368	0.292	0.251	0.221	0.200	0.202	0.193	0.181	0.137
-0.7	0.366	0.289	0.249	0.220	0.200	0.215	0.208	0.198	0.144
-0.8	0.366	0.286	0.249	0.222	0.205	0.234	0.229	0.221	0.152
-0.9	0.367	0.285	0.252	0.228	0.213	0.259	0.257	0.251	0.162
-1.0	0.367	0.285	0.258	0.237	0.226	0.293	0.294	0.291	0.175

Table 6 continued

Differential Elastic Cross Sections of Ni-60 ($\frac{\text{barns}}{\text{Sr}}$)

COS Ø c.m.	Energy (MeV)				
	2.0	2.5	3.0	3.5	4.0
1.0	1.007	1.178	1.322	1.474	1.712
0.9	0.769	0.862	0.934	0.992	1.117
0.8	0.580	0.617	0.640	0.646	0.700
0.7	0.431	0.431	0.423	0.403	0.416
0.6	0.317	0.293	0.268	0.239	0.230
0.5	0.230	0.194	0.162	0.133	0.114
0.4	0.166	0.126	0.093	0.068	0.049
0.2	0.089	0.054	0.031	0.019	0.010
0.0	0.057	0.036	0.025	0.022	0.026
-0.2	0.052	0.041	0.039	0.040	0.048
-0.4	0.064	0.056	0.052	0.052	0.056
-0.5	0.076	0.065	0.057	0.054	0.053
-0.6	0.091	0.076	0.062	0.054	0.046
-0.7	0.113	0.091	0.068	0.052	0.038
-0.8	0.141	0.110	0.077	0.052	0.032
-0.9	0.179	0.136	0.092	0.056	0.035
-1.0	0.227	0.173	0.162	0.069	0.053

Table 7

Cr-52

E_n (MeV)	σ_t (b)	
	Measured KFK - 120	Calculated
0.5	3.27 ± 10%	3.27
0.8	2.80 ± 10%	3.01
1.0	2.76 ± 10%	3.11
1.5	3.10 ± 10%	3.38
2.0	4.14 ± 10%	3.52
2.5	3.6 ± 10%	3.55
3.0	3.7 ± 10%	3.54
3.5	3.76 ± 10%	3.49
4.0	3.80 ± 10%	3.43

	σ_e(b)	σ_{in}(b)
	3.27	-
	3.01	-
	3.15	-
	3.15	0.23
	2.83	0.69
	2.74	0.81
	2.68	0.86
	2.60	0.89
	2.57	0.86

Table 8

Calculated Cross Sections (barns) for Neutron Excitations of Cr-52

E_n (MeV)	Compound Elastic	Excited levels (MeV)			
		1.46	2.43	2.965	3.112
0.5	1.402	-	-	-	-
0.8	1.447	-	-	-	-
1.0	1.514	-	-	-	-
1.5	1.405	0.226	-	-	-
2.0	0.897	0.685	-	-	-
2.5	0.633	0.811	-	-	-
3.0	0.446	0.811	0.052	-	-
3.5	0.290	0.620	0.104	0.167	-
4.0	0.212	0.497	0.137	0.226	0.002

Table 9

Differential Elastic Cross Sections of Cr $\left(\frac{\text{barns}}{\text{Str}}\right)$

cos ø c.m.	Energy (MeV)								
	0.5	0.8	1.0	1.5	2.0	2.5	3.0	3.5	4.0
1.0	0.525	0.629	0.744	1.020	1.216	1.412	1.583	1.697	1.788
0.9	0.471	0.530	0.607	0.780	0.886	0.991	1.068	1.112	1.142
0.8	0.424	0.448	0.496	0.591	0.632	0.673	0.693	0.697	0.695
0.7	0.383	0.380	0.406	0.445	0.440	0.440	0.429	0.413	0.397
0.6	0.347	0.325	0.334	0.334	0.299	0.276	0.251	0.227	0.207
0.5	0.317	0.280	0.278	0.251	0.200	0.166	0.137	0.114	0.096
0.4	0.290	0.243	0.233	0.191	0.134	0.097	0.071	0.052	0.040
0.2	0.246	0.189	0.171	0.122	0.069	0.043	0.030	0.022	0.020
0.0	0.213	0.154	0.136	0.094	0.058	0.048	0.046	0.047	0.051
-0.2	0.190	0.134	0.119	0.092	0.068	0.068	0.072	0.075	0.078
-0.4	0.176	0.130	0.122	0.106	0.085	0.082	0.083	0.082	0.081
-0.5	0.173	0.136	0.132	0.121	0.096	0.086	0.082	0.076	0.072
-0.6	0.174	0.148	0.149	0.142	0.108	0.089	0.077	0.065	0.058
-0.7	0.178	0.167	0.176	0.172	0.125	0.094	0.072	0.053	0.042
-0.8	0.187	0.195	0.214	0.214	0.149	0.104	0.070	0.043	0.029
-0.9	0.201	0.235	0.266	0.271	0.183	0.122	0.076	0.042	0.026
-1.0	0.221	0.289	0.335	0.349	0.233	0.155	0.097	0.057	0.042

Table 10

U-238

E_n (Mev)	σ_t (b)	
	BNL - 325	Calculated
0.475	7.6 ± 10%	6.60
0.57	7.2 ± 10%	6.55
0.60	7.1 ± 10%	6.55
0.65	7.0 ± 10%	6.55
0.72	6.8 ± 10%	6.56
0.77	6.7 ± 10%	6.58
1.10	6.5 ± 10%	6.73
1.17	6.6 ± 10%	6.77
1.50	6.70± 10%	6.94
2.0	6.9 ± 10%	7.02
2.5	7.0 ± 10%	6.99
3.0	7.5 ± 10%	6.79
3.5	7.8 ± 10%	6.44
4.0	7.7 ± 10%	6.01

σ_e (b)	σ_{in} (b)
5.09	1.51
4.97	1.58
4.96	1.59
4.96	1.59
4.98	1.58
5.02	1.56
5.27	1.46
5.36	1.41
5.72	1.22
6.04	0.98
6.07	0.92
5.86	0.93
5.51	0.93
5.08	0.93

Table 11

Calculated Cross-Sections (barns) for Neutron Excitations of U-238

		Excited levels (MeV)											
E_n (Mev)	Compound Elastic	0.045	0.148	0.308	0.651	0.71	0.728	0.935	0.986	1.03	1.11	1.13	1.17
.475	1.155	1.415	.093	-	-	-	-	-	-	-	-	-	-
.570	0.964	1.448	.138	-	-	-	-	-	-	-	-	-	-
.60	0.910	1.444	.143	-	-	-	-	-	-	-	-	-	-
.65	0.851	1.428	.158	-	-	-	-	-	-	-	-	-	-
.72	0.749	1.345	.169	-	0.063	0.007	-	-	-	-	-	-	-
.77	0.698	1.306	.177	-	.067	.01	-	-	-	-	-	-	-
1.10	.314	.661	.118	-	.062	.027	0.002	.174	.221	.195	-	-	-
1.17	.271	.565	.100	-	.059	.029	0.003	.169	.230	.209	-	-	-
1.50	.147	.324	.075	.002	.052	.039	0.008	.131	.235	.221	.093	.024	.021
2.0	.075	.176	.052	.004	.047	.052	.016	.084	.181	.180	.104	.041	.040
2.5	.054	.132	.056	013	.047	.077	.088	.058	.137	.137	.091	.044	.044

Table 12

Differential Elastic Cross-Sections of U-238 ($\frac{\text{barns}}{\text{Sr}}$)

cos Ø c.m.	E_n (M e v)									
	0.475	0.60	0.65	0.72	0.77	1.10	1.17	1.50	2.0	2.50
1.0	1.328	1.640	1.768	1.938	2.074	2.825	2.980	3.637	4.297	4.789
0.9	1.058	1.242	1.318	1.418	1.498	1.923	2.009	2.326	2.608	2.662
0.8	0.836	0.925	0.963	1.012	1.053	1.254	1.294	1.415	1.498	1.449
0.7	0.656	0.678	0.690	0.705	0.718	0.774	0.786	0.804	0.797	0.749
0.6	0.514	0.491	0.486	0.478	0.475	0.448	0.444	0.417	0.380	0.348
0.5	0.403	0.353	0.338	0.319	0.307	0.241	0.231	0.193	0.156	0.133
0.4	0.321	0.258	0.239	0.215	0.200	0.125	0.115	0.083	0.060	0.041
0.2	0.225	0.161	0.144	0.124	0.113	0.072	0.070	0.067	0.072	0.071
0.0	0.196	0.149	0.140	0.131	0.128	0.136	0.142	0.161	0.179	0.194
-0.2	0.211	0.183	0.180	0.180	0.183	0.214	0.223	0.248	0.261	0.259
-0.4	0.252	0.234	0.233	0.234	0.236	0.252	0.256	0.270	0.265	0.239
-0.5	0.278	0.260	0.258	0.256	0.255	0.249	0.248	0.250	0.235	0.209
-0.6	0.306	0.285	0.280	0.273	0.268	0.232	0.226	0.212	0.187	0.168
-0.7	0.335	0.309	0.300	0.284	0.274	0.203	0.191	0.160	0.129	0.116
-0.8	0.365	0.330	0.315	0.292	0.275	0.167	0.149	0.102	0.074	0.063
-0.9	0.396	0.351	0.330	0.297	0.273	0.129	0.107	0.050	0.042	0.052
-1.0	0.427	0.372	0.344	0.301	0.270	0.096	0.073	0.019	0.060	0.212

Table 13

Comparison Between Measured & Calculated Inelastic X-Sections
At .045 Mev

E_n (Mev)	σ_{in} (barns) (Measured)	σ_{in} (barns) (Calculated)
.475	1.32 ± .10	1.42
.570	1.44 ± .06	1.45
.60	1.26 ± .10	1.44
.650	1.20 ± .10	1.43
.77	1.14 ± .10	1.31
1.10	0.64 ± .16	0.66
1.17	0.75 ± .18	0.57

Table 14

Th - 232

E_n (Mev)	σ_t (b)		σ_e (b)	σ_{in} (b)
	BNL - 325	Calculated		
0.56	7.70 ± 10%	6.41	5.37	1.04
0.70	7.30 ± 10%	6.18	5.15	1.03
1.0	6.80 ± 10%	6.08	4.98	1.10
1.5	6.60 ± 10%	6.32	5.40	0.92
2.0	6.70 ± 10%	6.50	5.73	0.77
2.5	7.0 ± 10%	6.59	5.82	0.77
3.0	7.3 ± 10%	6.54	-	-
3.5	-	6.40		
4.0	-	6.16		

Table 15

Calculated Cross-Sections for Neutron Excitations of Th-232

		Excited levels (Mev)				
E_n (Mev)	Compound Elastic	.05	.163	.33	.725	.775
.56	.771	.957	.084	-	-	-
.70	.607	.917	.116	-	-	-
1.0	.231	.401	.710	-	.179	.191
1.5	.100	.205	.052	.002	.098	.173
2.0	.062	.142	.048	.004	.064	.137
2.5	.049	.126	.068	.024	.047	.113

Table 16

Differential Elastic Cross-Section

COS (C.M.)	En (M		
	.56	.70	1.0
1	1.4981	1.769	2.327
0.9	1.167	1.310	1.608
0.8	0.901	0.954	1.072
0.7	0.692	0.685	0.687
0.6	0.533	0.489	0.424
0.5	0.416	0.353	0.256
0.4	0.333	0.264	0.162
0.3	0.279	0.213	0.122
0.2	0.247	0.190	0.119
0.1	0.233	0.107	0.140
0.0	0.232	0.198	0.172
-0.1	0.240	0.216	0.207
-0.2	0.253	0.237	0.237
-0.3	0.269	0.256	0.259
-0.4	0.285	0.272	0.268
-0.5	0.299	0.283	0.263
-0.6	0.311	0.287	0.245
-0.7	0.320	0.205	0.216
-0.8	0.326	0.278	0.179
-0.9	0.328	0.267	0.139
-1.0	0.330	0.254	0.101

us of Thorium 232 ($\frac{\text{barns}}{\text{Sr}}$)

lev)

1.5	2.0	2.5
3.233	3.904	4.432
2.069	2.373	2.484
1.259	1.361	1.359
0.717	0.721	0.700
0.376	0.342	0.318
0.183	0.142	0.114
0.092	0.617	0.034
0.072	0.554	0.036
0.094	0.909	0.086
0.138	0.145	0.153
0.189	0.202	0.215
0.237	0.248	0.255
0.271	0.279	0.269
0.288	0.289	0.262
0.284	0.276	0.241
0.260	0.242	0.212
0.219	0.193	0.173
0.165	0.135	0.124
0.106	0.081	0.683
0.532	0.050	0.056
0.214	0.069	0.241

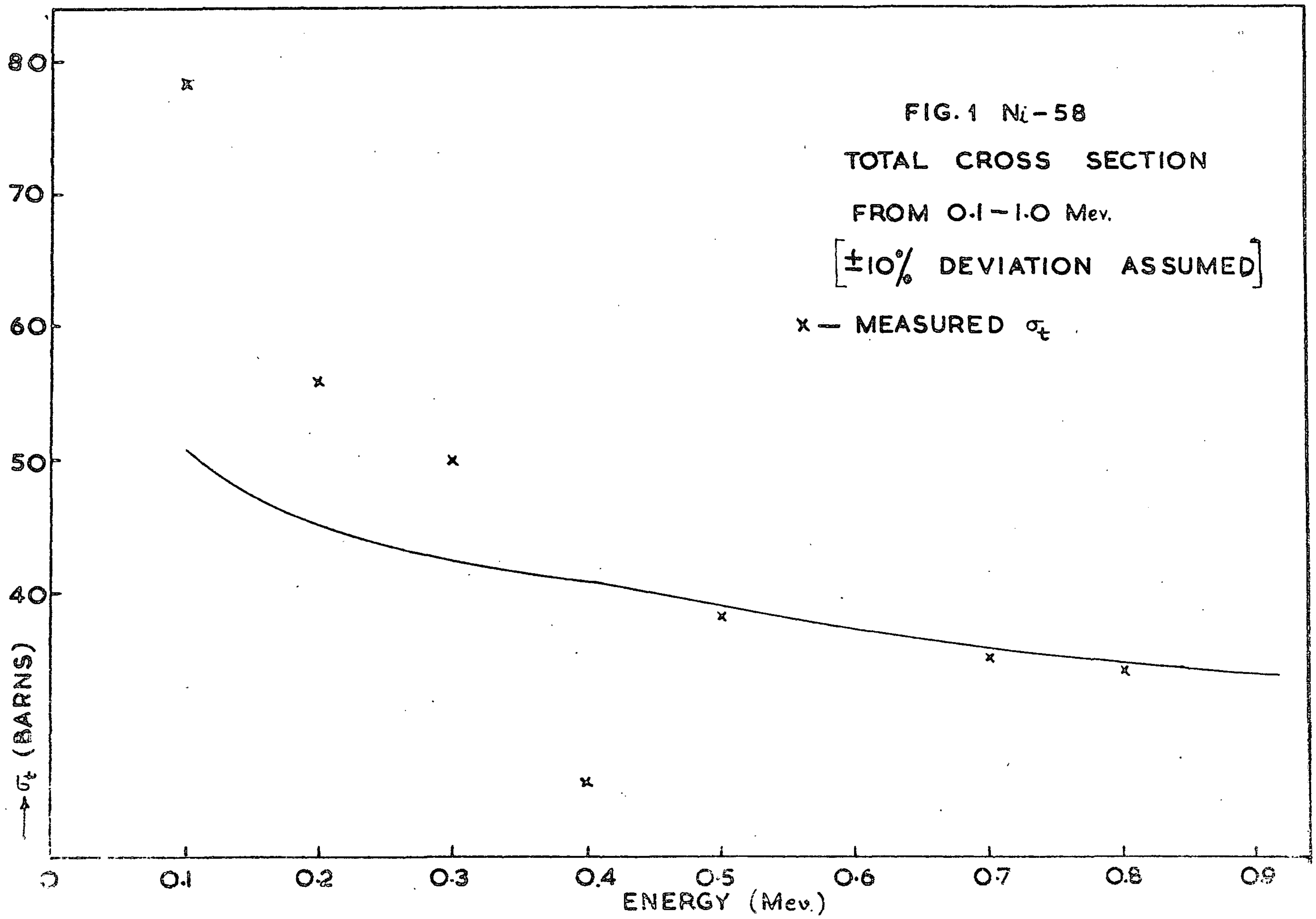

FIG. 1 Ni-58
TOTAL CROSS SECTION
FROM 0·1–1·0 Mev.
[±10% DEVIATION ASSUMED]
x — MEASURED σ_t
80
70
60
50
40
σ_t (BARNS)
0
0·1
0·2
0·3
0·4
0·5
0·6
0·7
0·8
0·9
ENERGY (Mev.)

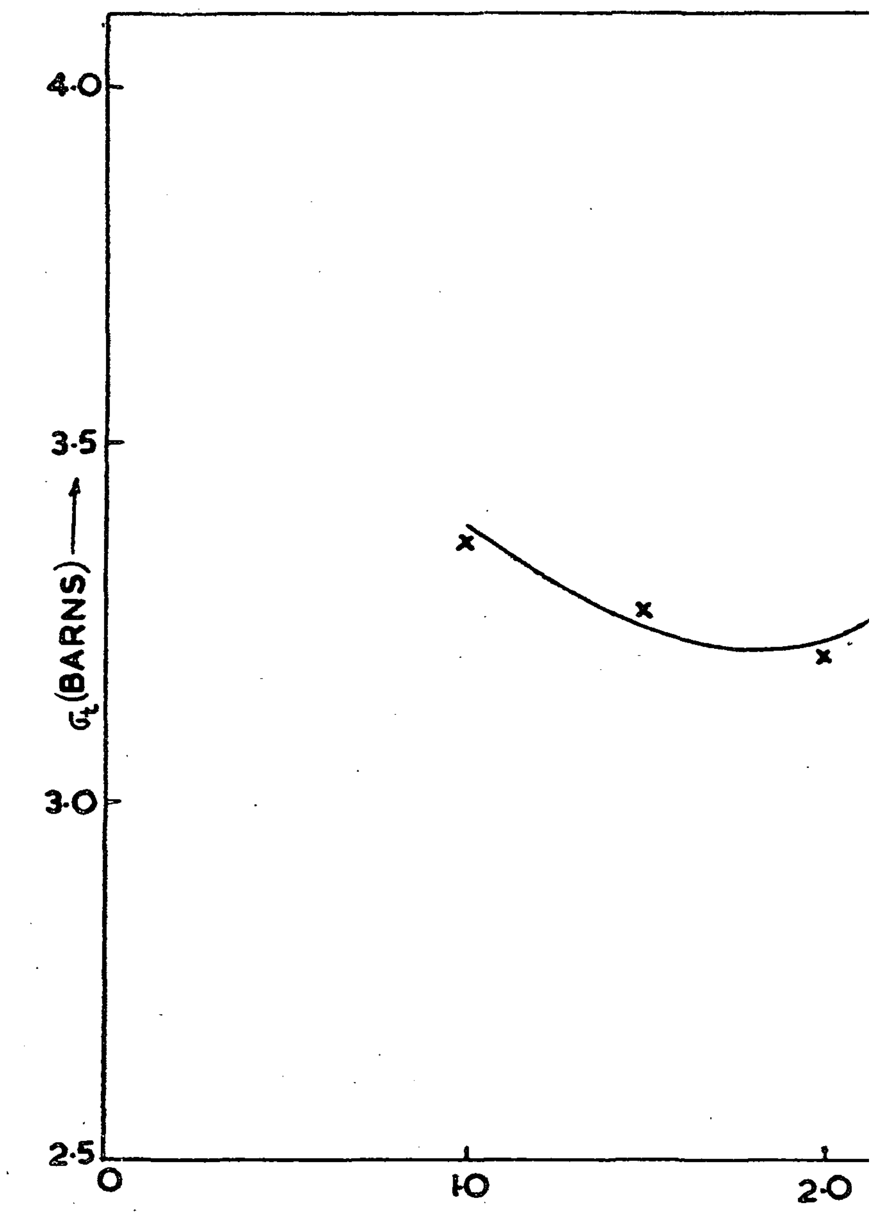

4·0
3·5
3·0
2·5
σ_t (BARNS)
0
1·0
2·0

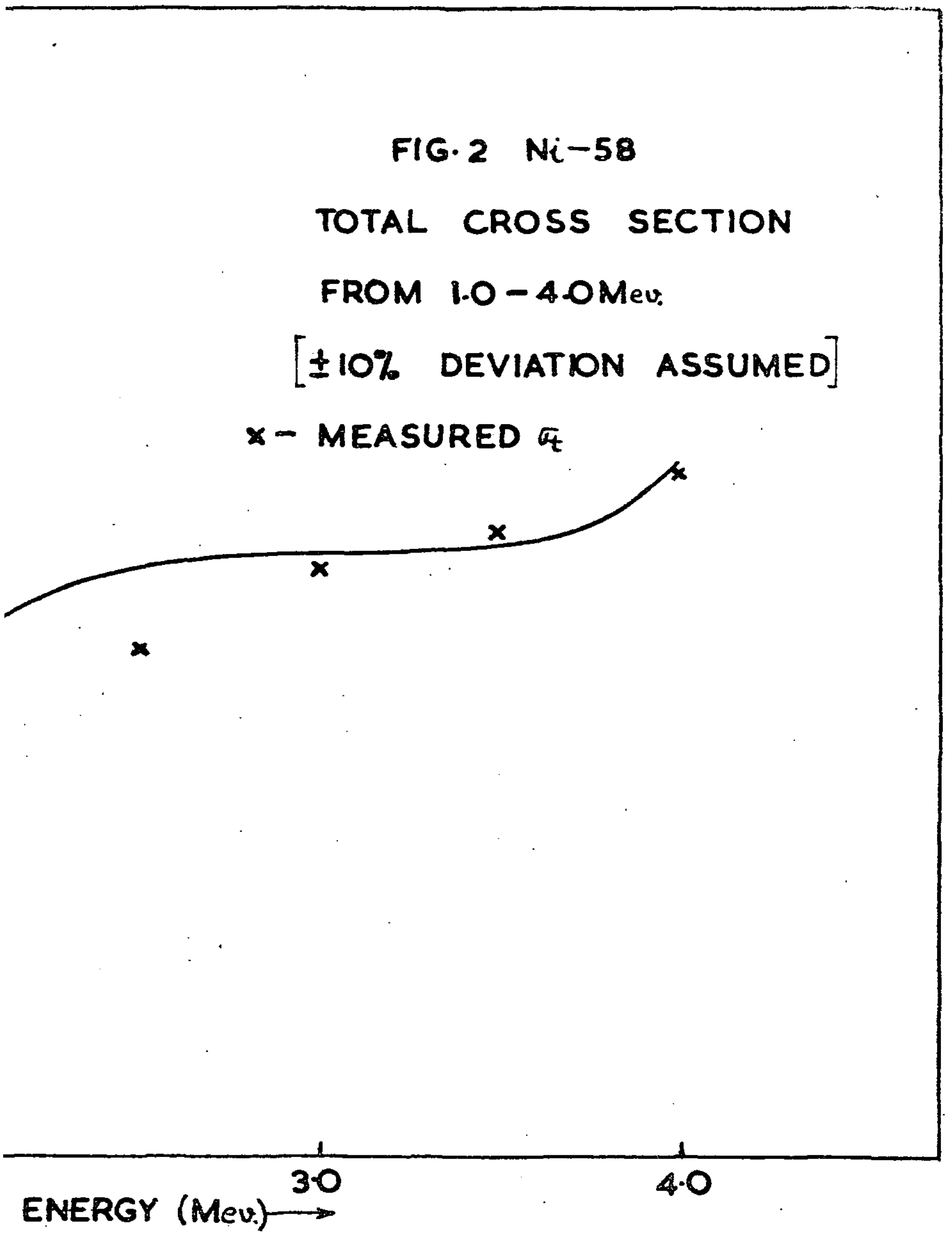

FIG· 2 Ni–58
TOTAL CROSS SECTION
FROM 1·0 – 4·0 Mev.
[± 10% DEVIATION ASSUMED]

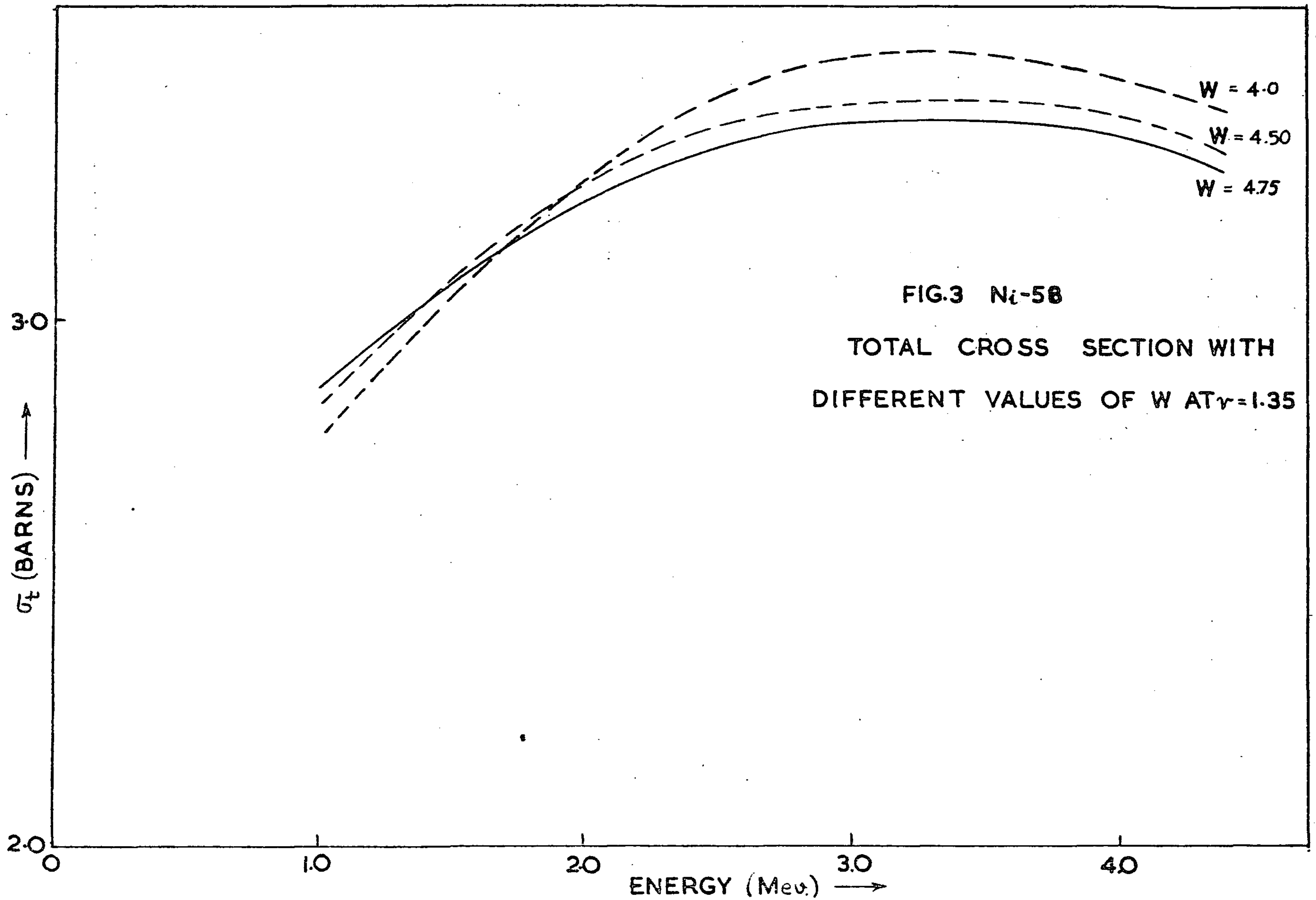
W = 4.0
W = 4.50
W = 4.75
FIG.3 Ni-58
TOTAL CROSS SECTION WITH
DIFFERENT VALUES OF W AT r = 1.35
3.0
2.0
0
1.0
2.0
3.0
4.0
ENERGY (Mev.)
σt (BARNS)

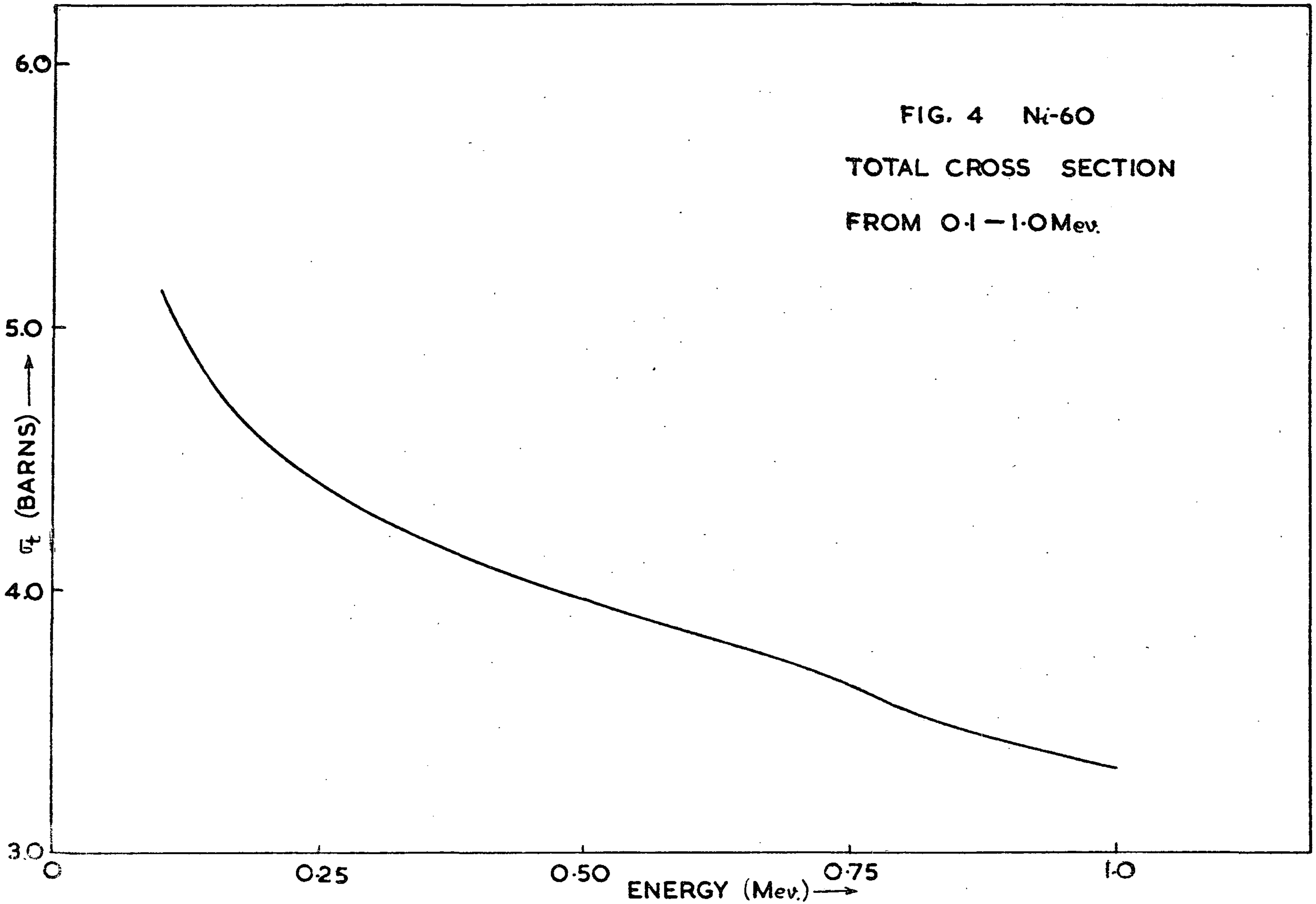

FIG. 4 Ni-60
TOTAL CROSS SECTION
FROM 0·1 — 1·0 Mev.
6.0
5.0
4.0
3.0
σt (BARNS)
0
0·25
0·50
0·75
1·0
ENERGY (Mev.)

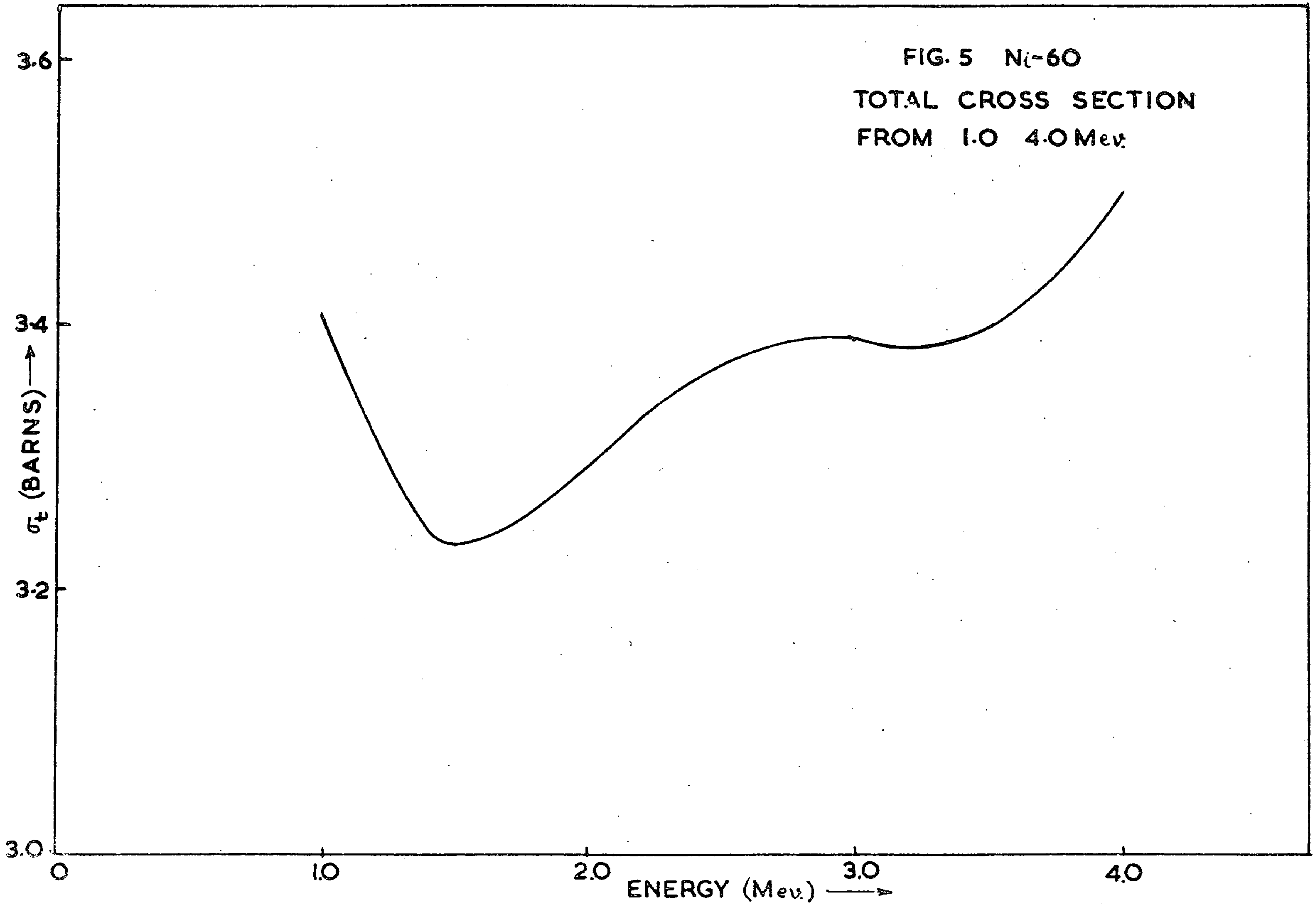

FIG. 5 Ni-60
TOTAL CROSS SECTION
FROM 1.0 4.0 Mev.

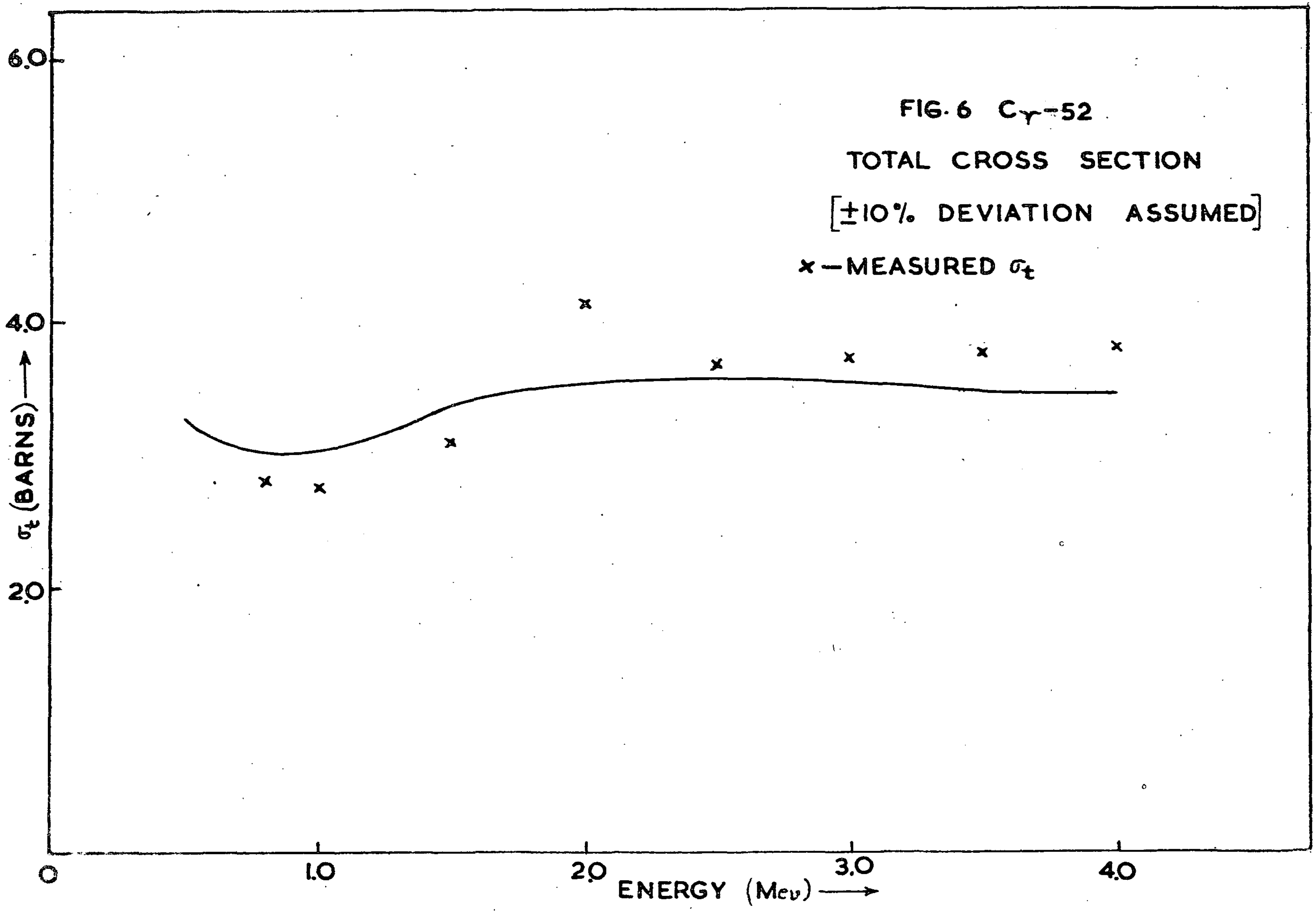

FIG. 6 Cr-52
TOTAL CROSS SECTION
[±10% DEVIATION ASSUMED]
× — MEASURED σ_t
σ_t (BARNS) →
6.0
4.0
2.0
0
1.0
2.0
3.0
4.0
ENERGY (Mev) →

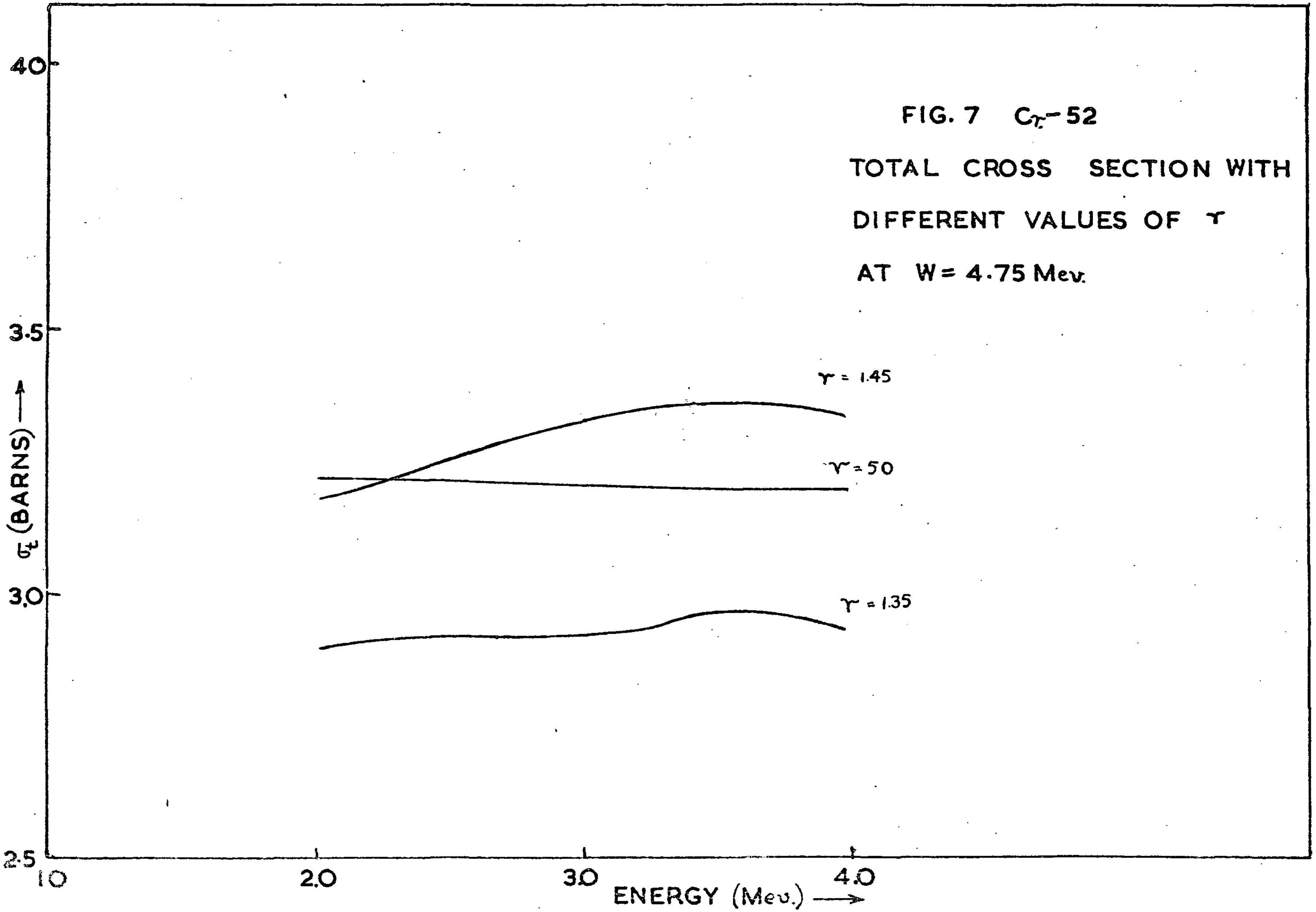

FIG. 7 Cr-52

TOTAL CROSS SECTION WITH DIFFERENT VALUES OF τ AT W = 4.75 Mev.